

# Development of alkaline electrochemical characteristics demonstrates soil formation in bauxite residue undergoing natural rehabilitation

by Kong, X., Tian, T., Xue, S., Hartley, W., Huang, L., Wu, C. and Li, C.

**Copyright, Publisher and Additional Information:** This is the author accepted manuscript. The final published version (version of record) is available online via Wiley. Please refer to any applicable terms of use of the publisher.

DOI: <https://doi.org/10.1002/ldr.2836>



Kong, X., Tian, T., Xue, S., Hartley, W., Huang, L., Wu, C. and Li, C. 2017. Development of alkaline electrochemical characteristics demonstrates soil formation in bauxite residue undergoing natural rehabilitation. *Land degradation and Development*.

26 October 2017

1     **Development of alkaline electrochemical characteristics improves land degraded**  
2                                    **by bauxite Residue**

3             Xiangfeng Kong <sup>1,2</sup>, Chuxuan Li <sup>1,2</sup>, Shengguo Xue <sup>1,2,\*</sup>, William Hartley <sup>3</sup>, Xiaofei Li <sup>1,2</sup>,

4                                    Yiwei Li <sup>1,2</sup>

5     <sup>1</sup> School of Metallurgy and Environment, Central South University, 932 Lushan South Road, Changsha, Hunan, 410083, PR China

6     <sup>2</sup> Chinese National Engineering Research Center for Control & Treatment of Heavy Metal Pollution, Central South University,  
7                                    Changsha, 410083, PR China

8     <sup>3</sup> Crop and Environment Sciences Department, Harper Adams University, Newport, Shropshire, TF10 8NB, United Kingdom

9                                    **ABSTRACT**

10    Bauxite residue (BR) is a highly alkaline hazardous waste produced from alumina extraction processing,  
11    and has a complex mineralogy, which gives rise to soil basification and land degradation. Current  
12    management practices have mainly focused on containment, with less attention given to long-term natural  
13    evolution of its physical and chemical properties, particularly surface electrochemical characteristics.  
14    Weathering appears to reduce its environmental impact and alleviate its effect on land degradation whilst  
15    potentially providing opportunities for surface revegetation, improved soil-formation and hence land  
16    development of bauxite residue disposal areas (BRDAs). Natural evolution of mineralogy, zeta potential,  
17    isoelectric point (IEP), surface protonation and active alkaline groups are investigated here. Alkaline  
18    minerals of calcite, hydrogarnet and sodalite were slowly transformed or dissolved and their  
19    concentrations reduced with increasing duration following disposal. Amorphous and semi-amorphous  
20    minerals also decreased with a corresponding decrease in BET surface area and sorption sites. Zeta  
21    potential curves of the fresh residue had more slope during potentiometric titration, whilst for aged  
22    residue these became shallower with disposal duration. The IEP of fresh residue was significantly higher  
23    ( $P < 0.05$ ), and the IEPs of aged residues were significantly lower ( $P < 0.05$ ) with a significant decrease  
24    of IEP with increasing disposal time. Transformation of alkaline minerals, improvement of the poorly  
25    crystalline structure, and precipitation of amorphous and semi-amorphous minerals, decreased surface  
26    protonation and surface active alkaline groups with disposal duration, benefiting decision making with  
27    regards to soil formation and further land development of BRDAs.

28  
29    KEYWORDS: Bauxite residue; natural evolution; alkalinity; isoelectric point; alkaline groups

30  
31  
32  
33  
34  
35  

---

\*Corresponding author. Tel: + 86 731 85552958

E-mail address: sgxue70@hotmail.com (S.G. Xue); sgxue@csu.edu.cn

37 Land degradation is costly to human progress as a result of mismanagement of natural capital (Costanza  
38 *et al.*, 2014; Sutton *et al.*, 2016). Increasing demand for accessible productive land therefore requires the  
39 remediation and improvement of degraded land. Bauxite mining is well-known for its aggressive mining  
40 activities, producing large tailings, particularly of bauxite processing residues, which degrade large tracts  
41 of land and cause multiple environmental problems that currently restrict the sustainable development of  
42 the alumina industry (Gelencser *et al.*, 2011; Mayes *et al.*, 2016; Goloran *et al.*, 2017; Kong *et al.*, 2017a).  
43 Bauxite residue (BR), or red mud, is an alkaline solid waste produced during alumina extraction from  
44 bauxite, with approximately 0.5-2 tons of residue generated per ton of alumina product (Grafe *et al.*,  
45 2011; Evans *et al.*, 2016). Currently, the accumulative inventory of bauxite residue has reached over 4  
46 billion tons, and is still increasing rapidly (Liu & Naidu, 2014; Ye *et al.*, 2014; Kinnarinen *et al.*, 2015).  
47 The management of bauxite residue is a seriously challenging waste problem that is a major concern to  
48 alumina refineries. Globally, there is no economic alternative to landfill, therefore almost all bauxite  
49 residue continues to be stored indefinitely in land-based BRDAs (Burke *et al.*, 2013; Xue *et al.*, 2016a;  
50 Zhu *et al.*, 2016a). The liabilities and environmental risks including freshly formed alkaline dust and  
51 efflorescence, leaching of caustic liquor, degradation of surrounding land and trace metal and remediation  
52 costs (Liu *et al.*, 2014; Samal *et al.*, 2015; Buckley *et al.*, 2016; Santini & Banning, 2016; Higgins *et al.*,  
53 2016; Xue *et al.*, 2016b; Higgins *et al.*, 2017) have all afforded incentives to find selectable management  
54 and treatment options.

55 The majority of the residues mineralogy is derived from weathering of bauxite and parent rock, but the  
56 bauxite digestion process also produces secondary minerals, especially desilication products of  
57 aluminosilicates such as cancrinite, sodalite and hydrogarnet, but also oxides, carbonates, and hydroxides  
58 (Grafe *et al.*, 2011; Palmer & Frost, 2011). The majority of calcium (Ca) and all the sodium (Na) present  
59 are introduced from the caustic soda (NaOH) and lime (CaO) added during alumina extraction and NaOH  
60 regeneration. Formations of cancrinite ( $[\text{Na}_6\text{Al}_6\text{Si}_6\text{O}_{24}] \cdot 2[\text{CaCO}_3]$ ), sodalite ( $[\text{Na}_6\text{Al}_6\text{Si}_6\text{O}_{24}] \cdot [2\text{NaX}$  or  
61  $\text{Na}_2\text{X}]$ ), and other aluminosilicates are generated predominately during digestion (Freire *et al.*, 2012; Pan  
62 *et al.*, 2015). These are fine grain sized and structurally complex combined with high sodicity and soluble  
63 alkalinity. Furthermore, Ca minerals are commonly produced during caustic regeneration with calcium  
64 hydroxide precipitating carbonate alkalinity (Pan *et al.*, 2015; Xue *et al.*, 2016a). Subsequently these  
65 minerals appear as alkaline minerals in bauxite residue.

66 Currently, research has focused on conversion of the high alkalinity of bauxite residue prior to disposal  
67 and as an amelioration technique for encouraging revegetation and further land development (Xue *et al.*,  
68 2016a; Kong *et al.*, 2017b). Seawater neutralization, waste acid dosing, gypsum transformation and  
69 carbon dioxide sequestration are often used to ameliorate its alkalinity, but nevertheless, there still  
70 remains insufficient long-term success as a result of economics and side effects (Wong & Ho, 1993;  
71 Wong & Ho, 1994; Tuazon & Corder, 2008; Sushil & Batra, 2012; Couperthwaite *et al.*, 2013; Rai *et al.*,  
72 2013; Clark *et al.*, 2015; Jones *et al.*, 2015; Kishida *et al.*, 2016). Furthermore, such methods have only  
73 concentrated on artificial amelioration of alkaline substances with less attention being given to natural  
74 development of alkalinity and its occurrence in bauxite residue disposal areas (BRDAs).

75 The natural change in behavior of alkalinity in the residue is primarily governed by electric charge;  
76 positively charged cations are attracted to negatively charged surfaces, and negatively charged anions are  
77 attracted to positively charged surfaces. This opposite attraction could be determined by the zeta potential

78 ( $\zeta$ ), and is dependent on pH (Castaldi *et al.*, 2010; Liu *et al.*, 2013; Kosmulski, 2014). The pH in which  
79 surface charge is efficiently balanced, is the surface charge density and the electroacoustic isoelectric  
80 point (IEP), and is influenced by the electro and/or surface chemistry of the complexity of mineralogy and  
81 the various hydrolysable surface groups (Kairies *et al.*, 2005; Wang *et al.*, 2008; Freire *et al.*, 2012).

82 There is limited mechanistic understanding of bauxite residue surface electrochemical characteristics  
83 following its long term disposal. Certainly, a lack of understanding of development of electrochemical  
84 chemistry and its effects on alkalinity behavior, has been highlighted as a significant knowledge gap with  
85 special reference to the safe management, revegetation, soil formation and inhibition of land degradation  
86 in BRDAs (Grafe *et al.*, 2011; Liu *et al.*, 2013; Kong *et al.*, 2017b). This study therefore had the  
87 following specific objectives: (1) to discuss the transformation in alkaline mineralogy within bauxite  
88 residue following long term natural disposal, and (2) to investigate the zeta potential, isoelectric point,  
89 surface protonation and alkaline groups of bauxite residue, and to characterize the natural evolution of  
90 surface chemical characteristics.

## 91 MATERIALS AND METHODS

### 92 *Field sampling and sample preparation*

93 The bauxite residue sample used in this study was collected at the bauxite residue disposal area (BRDA)  
94 of the Zhongzhou refinery, Aluminum Corporation of China, Jiaozuo city, Henan province, China.  
95 Samples were collected from 5 locations as follows; freshly deposited residue (0 years) (Lat 35°24'3.76"  
96 N, Long 113°25'38.18" E), 5 year old residue (5) (Lat 35°24'3.03" N, Long 113°25'38.82" E), 10 year old  
97 residue (10) (Lat 35°24'2.43" N, Long 113°25'38.26" E), 15 year old residue (15) (Lat 35°24'1.86" N,  
98 Long 113°25'40.39" E) and 20 year old residue (20) (Lat 35°24'28.11" N, Long 113°25'47.33" E).  
99 Residue age differences are approximate, but were determined due to a change in zonation which was  
100 clearly visible within the stacks. At each location, three sub-samples (0-30 cm sampling depths) were  
101 collected having a distance of 5 meters from each other to form a representative sample. Samples were  
102 respectively deposited in polyethylene bags, returned to the laboratory and subsequently air-dried for 5  
103 days, slightly disaggregated using a mortar and pestle, and sieved to retain the <2 mm fraction. Two  
104 stages of water washing were conducted to remove soluble alkalinity and/or salt. Samples were mixed  
105 with ultrapure water with a vortex mixer (adequate mixing) for two stages of 5 min to insure dissolution  
106 of the maximum soluble alkaline minerals and/or salts. Subsequently the suspension was centrifuged at a  
107 low speed (4000 rpm for 15 min), and residual solids were naturally dried for 2 days, afterwards dried at  
108 60 °C for 96 h. The fully dried solids were slightly crushed in a mortar to disaggregate, and sieved to  
109 retain the <48  $\mu\text{m}$  fraction.

### 110 *Sample characterization*

111 Bauxite residue samples for X-ray powder diffraction (XRD) analysis were conducted on a Bruker D8  
112 discover 2500 with a Cu  $K\alpha_1$  tube using a Sol-X detector. X-ray diffraction patterns were collected from  
113 10 to 80° at a 0.04°  $2\theta$  step size and a 1°  $2\theta$  min<sup>-1</sup> scan rate. The PANalytical analysis package was  
114 applied to identify and quantify phases from XRD data. The relative intensity of the method was used to  
115 quantitatively calculate mineral phases. The value of the reference intensity ratio ( $RIR_i$ ) of the reference  
116 code corresponding to phase  $i$  is directly determined, and the area  $I_i$  of maximum intensity peak of the  
117 phase  $i$  is calculated. Then, the weight fraction  $W_i$  is calculated from  $W_i = (I_i/RIR_i) / (\sum_i^n I_i/RIR_i)$ .

118 Amorphous and semi-amorphous minerals of each sample was estimated with the aid of Jade v.7  
119 software. The BG-Offset parameter shifts was used to fit an appropriate background, where the peaks  
120 above this were integrated, then the whole integrated area provides a proportion of crystalline material.  
121 Semi-amorphous materials were evaluated by identifying the area between the complex higher-order  
122 background (BG) and a simple first-order BG for peak fitting by means of weighted integration.  
123 Subsequently, the whole weighted area was subtracted from this determined area. The simple first-order  
124 background, and the diffraction pattern profile were deleted, then diffraction pattern was divided on a 5  
125 decimal equal place. This area between the simple first-order BG and the complex peak fitting BG was  
126 cut off, and the two regions were respectively weighed, finally quantifying the semi-amorphous minerals.

127 Specific surface area (BET) of dried residues were performed on a Quantachrome Quadrasorb S1-3MP  
128 auto-adsorption analyzer (employing liquid nitrogen adsorption) with the static volumetric technique  
129 (using  $t$  method). Liquid nitrogen was equilibrated with solid powder samples for 20 seconds, followed  
130 by degassing 20 min. Subsequently, samples were sequentially degassed at 150 °C for 1 h at 0.02 - 0.2  
131 atm pressures ( $P/P_0$ ). Qswin analysis software was used to analyze adsorption isotherm to determine the  
132 BET.

133 Scanning electron microscopy (SEM) of bauxite residue samples were observed on a Netherlands FET  
134 Quanta-200. Samples were paved on a Cu support plate filmed with Au (conductive coating), then  
135 deposited by low vacuum sputter coating, and subsequently examined by a GSED field emission probe.

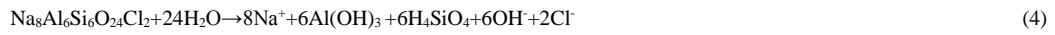
#### 136 *Isoelectric point determination*

137 The isoelectric point (IEP) of bauxite residue was measured by potentiometric titration using ultrasonic  
138 attenuation and electro-sonic acoustics in a Colloid Dynamics Acoustizer II. All three replicates of the 5  
139 different aged residues were respectively dispersed at 2.5 % (mass fraction) in a 0.001 mol L<sup>-1</sup> NaCl  
140 electrolyte (Freire *et al.*, 2012). Then, samples were dispersed in an ultrasonic cell crusher noise-isolating  
141 chamber for 30 min, then rested for 10 min. The electrolyte pH was normalized to pH 10 from its initially  
142 resting pH (approximately 11-9) prior to introduction into the Acoustizer II. Immediately, samples were  
143 stirred at 150 rpm for 3 min, forming a homogeneous suspension. Subsequently, a potentiometric titration  
144 was proceeded from pH 10 to 5 with 0.1 mol L<sup>-1</sup> HCl at 0.5 pH unit decrements.

## 145 RESULTS AND DISCUSSION

#### 146 *Mineralogy*

147 The quantitative phases of bauxite residue obtained by PANalytical analysis from XRD data reveal phase  
148 transformations during the residues long-term disposal (Table I). The alkaline phases from the freshly  
149 stored bauxite residue were calcite (CaCO<sub>3</sub>), cancrinite (Na<sub>8</sub>Al<sub>6</sub>Si<sub>6</sub>O<sub>24</sub>(CO<sub>3</sub>)(H<sub>2</sub>O)<sub>2</sub>), hydrogarnet  
150 (Ca<sub>3</sub>Al<sub>2</sub>(SiO<sub>4</sub>)<sub>x</sub>(OH)<sub>12-4x</sub>), sodalite (Na<sub>8</sub>Al<sub>6</sub>Si<sub>6</sub>O<sub>24</sub>Cl<sub>2</sub>) and tri-calcium aluminate (Ca<sub>3</sub>Al<sub>2</sub>(OH)<sub>12</sub>), whilst a  
151 range of Al hydroxide ( $\alpha$ -AlOOH), Fe oxide ( $\alpha$ -Fe<sub>2</sub>O<sub>3</sub>), a Ti mineral (Ca(TiO<sub>3</sub>)) and Si oxide (SiO<sub>2</sub>) were  
152 also identified (Figure 1). The quantitative XRD results (Table I) indicate that the freshly stored residue  
153 contained 49.1 % alkaline minerals, originating from alumina extraction processes (Bayer, sinter and  
154 combined process), the bauxite source (gibbsite, diaspore and boehmite), digestion conditions and CaO  
155 addition (Liao *et al.*, 2015). The mineral characteristics of calcite, cancrinite, hydrogarnet, sodalite and  
156 tri-calcium aluminate are fundamental to the residues high alkalinity, and the following dissolution  
157 reactions of these buffering alkaline solids are summarized as Eqs. 1-5.



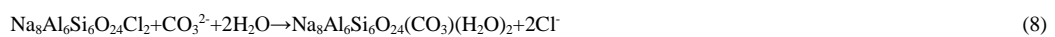
159

160 Hydrogarnet is the primary alkaline mineral (Table I) and quantification reveals that this mineral was  
 161 gradually dissolved and converted to stable gibbsite (Eq. 3) due to its persistent dissolution characteristics  
 162 (Santini *et al.*, 2015b). For fresh bauxite residue, the calcite concentration was 10.0 %, compared to 8.2 %  
 163 in the 20 year old residue. Transformation of calcite was relatively slow compared to those of acid, CO<sub>2</sub>  
 164 and heat treated bauxite residues (Genç-Fuhrman *et al.*, 2004; Sharif *et al.*, 2011; Yang *et al.*, 2012; Zhu  
 165 *et al.*, 2015). Results here suggest that during time from disposal, calcite minerals were partly dissolved  
 166 (approximately 2 %). The dissolved calcite was more than 2 % due to formation and precipitation of fresh  
 167 calcite (Eqs. 6 and 7). Sodalite concentration also decreased with increasing time from disposal whilst its  
 168 concentration in the 20 year old disposed residue reduced by 20 %. During disposal, sodalite was slowly  
 169 transformed to cancrinite (Eq. 8) (Barnes *et al.*, 1999; Gatta *et al.*, 2016), slightly increasing the cancrinite  
 170 concentration in the 20 year old residue. However, there was no obvious change to cancrinite until this  
 171 period (Table I), and may be attributed to its dissolution (Eq. 2) during time from disposal. Tri-calcium  
 172 aluminate dissolved more slowly than other buffering alkaline minerals. The majority of tri-calcium  
 173 aluminate was stable (its concentration maintained at about 3.3 %) during disposal, which is consistent  
 174 with the transformation mechanisms described elsewhere (Hawkins & Roy, 1963; Tsuchida, 2000; Gong  
 175 *et al.*, 2003). Transformations of hydrogarnet, cancrinite and sodalite resulted in an increasing  
 176 concentration of gibbsite (Table I). The gibbsite to diaspore transformation is well-known (Murray *et al.*,  
 177 2009; Santini *et al.*, 2015b), naturally increasing diaspore concentrations in the aged residues. Results  
 178 indicate that the concentration of diaspore was maintained at approximately 6.0 %, suggesting that the  
 179 transformation of gibbsite to diaspore was not activated through natural conditions (Table I).

180



Where present, Ca<sup>2+</sup> and OH<sup>-</sup> mainly come from the dissolution reactions of hydrogarnet and tri- calcium  
 aluminate (Eqs. 3 and 5).



181

182 Furthermore, XRD results (Table I and Figure 1) reveal a large quantity of hematite (approximately  
 183 26 %) in the different aged residues. Hematite concentrations had no obvious change. Hematite remained  
 184 constant in the aged residues because its transformation required acidic conditions (pH 4 to 5) (Snars &  
 185 Gilkes, 2009; Jones *et al.*, 2015;), and was therefore limited by the buffering action of the alkaline solids.  
 186 Perovskite and quartz minerals were also stable (Table I). Results indicate that perovskite and quartz are  
 187 not affected by weathering even after 20 years.

188

189 XRD results also show a large proportion of amorphous and semi-amorphous minerals in the different  
 190 aged residues. Following disposal, concentrations of these minerals decreased with a corresponding  
 decrease in BET surface area (Table I). A similar trend was attributed to reduced metal and oxyanion

191 binding on sorption sites of hematite (Genc-Fuhrman *et al.*, 2004; Smičiklas *et al.*, 2014). Additionally,  
192 these minerals with structural defects further influence sorption behavior, since mineral porosity and  
193 structural defects determine intraparticle diffusion which allow the surface adsorbed ions to re-distribute  
194 (Davis & Kent, 1990; Axe & Trivedi, 2002; Castaldi *et al.*, 2008; Clark *et al.*, 2009; Clark *et al.*, 2011).  
195 With increasing time from disposal, sorption sites decreased (Table I) whilst intraparticle diffusion  
196 decreased ion binding, filling in the surface charge to release ions.

#### 197 *Zeta potential curves and isoelectric point*

198 Zeta potential curves from the different aged residues (Figure 2) reveal that for fresh residue more slope  
199 exists during the potentiometric titration (zeta potential changed from 27.7 mV to -27.9 mV at pH range  
200 of 5-10). For the older residue (20 years) the zeta potential curve has a shallower slope, changing from 17  
201 mV to -17.8 mV at the same pH range. The trends of the 5, 10 and 15 year old residues were between that  
202 of the fresh and 20 year old residue. Before titration, the soluble alkalinity may have been removed during  
203 the two stages of water washing. Changes to the curves suggest that concentrations of alkaline minerals  
204 (hydrogarnet, calcite, sodalite) (Table I) may contribute to control the sloped tendency of the curve. The  
205 fresh residue that contained a higher concentration of alkaline materials (49.1 %, Table I), had a higher  
206 zeta potential (Figure 2). The alkaline concentrations of the aged residues decreased post disposal, and the  
207 zeta potentials were also considerably lower (Figure 2), further reflecting that transformations of  
208 hydrogarnet, calcite and sodalite over time. Following disposal, concentrations of amorphous and  
209 semi-amorphous minerals decreased (Table I), as did the zeta potentials (Figure 2), suggesting that these  
210 materials may be responsible for the slope of the curves. In addition, the fresh residue that was composed  
211 of 0.1-0.5  $\mu\text{m}$  particles in 5-10  $\mu\text{m}$  aggregates was poorly-crystallized, relatively dispersed and disordered  
212 (Figure 3 A). During disposal, small particles were partly removed (Figure 3 B-C), which may have been  
213 leached by rainwater, whilst others formed new aggregates. The macro-aggregate particles of the aged  
214 residues increased and were regularly distributed (Figure 3 B-C). Particle results further suggest that fine  
215 grains decreased and macro-aggregates formed, providing a much shallower zeta potential curve, whilst a  
216 corresponding decrease in BET surface area occurred after disposal (Table I).

217 The isoelectric points of the different aged residues were calculated from the mean zeta potential  
218 curves (Figure 2) and statistical analysis (Figure 4). They indicate significant differences between the  
219 fresh and aged residues. A significant decrease in the IEP was clear with increasing time from disposal;  
220 the IEP of fresh residue was significantly higher ( $P \leq 0.05$ ), whilst the IEP of aged residues was  
221 significantly lower ( $P \leq 0.05$ ).

222 The fresh residue had a higher concentration of alkaline materials (hydrogarnet, calcite and sodalite)  
223 (Table I), which had a higher IEP (Figure 4), whilst the aged residues that contained a lower concentration  
224 of alkaline minerals, had a lower IEP (Figure 4). The difference in mineralogy between the fresh and aged  
225 residues was only in their concentrations (Table I), suggesting that the IEP is directly related to the  
226 content of alkaline minerals within residues. Transformation of calcite results showed that the dissolved  
227 products were  $\text{Ca}^{2+}$  and  $\text{CO}_3^{2-}$  (Eq. 1), where calcite appears to only weakly influence the IEP (similar to  
228 previous findings (Freire *et al.*, 2012)). Hydrogarnet and sodalite dissolved and formed orthosilicic acid  
229 polymers, which are unstable and slowly hydrolyzed, resulting in the precipitation of  $\text{SiO}_2$ . The newly  
230 formed  $\text{SiO}_2$  lowers the IEPs in the aged residues due to its lower IEP (approximately 2)  
231 (Jimenez-Angeles, 2012; Kosmulski, 2014). Additionally, the lower IEP in the aged residues may also be  
232 attributed to the changes of particle size distribution due to the decrease of fine grains and the formation

233 of macro-aggregates (Figure 3), which further verify the corresponding decrease of BET surface area post  
234 disposal.

#### 235 *Surface protonation and alkaline group*

236 The acid-base titration curves (Figure 5) reflect the clear distinction of acid adsorption to the surface of  
237 minerals within the residues following long-term disposal. The titration curve of the fresh residue  
238 provides a relatively shallower exchange curve, suggesting that the fresh residue produced increased  
239 protonation, particularly at low pH. The curves of the aged residues provide a steep exchange curve,  
240 indicating that the aged residues have limited adsorption of acid to their surfaces. In particular, the proton  
241 exchange curve of 20 year old residue is the steepest, reflecting that surface adsorption of H<sup>+</sup> may be a  
242 primary buffering agent. It appears that a reduction in alkaline mineral concentrations (Table I), together  
243 with the improvement of the crystalline structure (fine grains reduced and macro-aggregates formed,  
244 Figure 3) (Axe & Trivedi, 2002; Freire *et al.*, 2012), and precipitation of amorphous and semi-amorphous  
245 minerals (sorption sites reduced, Table I) during long-term disposal, may provide decreased surface  
246 protonation and acid neutralizing capacity.

247 The acid-base titration curves reveal a clear distinction of the extensively horizontal section (the  
248 distance between beginning location and end location) (Figure 5), which is governed by the proton's  
249 adsorption/desorption of the surface active alkaline groups of minerals within the residues following  
250 long-term disposal. The length of the horizontal region may reflect the concentration of these groups on  
251 the surface of minerals, and the natural evolution of the surface active alkaline groups (-OH) may be  
252 calculated and examined (Figure 6).

253 The surface active alkaline groups from the different disposal ages (Figure 6) indicate that alkaline  
254 groups exist on the surface of residue particles. During disposal, development of surface active alkaline  
255 groups provided some inconsistencies with increasing duration following disposal. For fresh residue, the  
256 initial alkaline group recorded was 1.02 mol H<sup>+</sup> kg<sup>-1</sup> solid and was significantly greater ( $P \leq 0.05$ ) (Figure  
257 6), which continuously consumed H<sup>+</sup> to some extent (a broad horizontal region shown in Figure 5) whilst  
258 maintaining a relatively constant pH. Fresh residue presents relatively abundant alkaline groups, but these  
259 significantly decrease in the aged residues, especially the 20 year old bauxite residue (0.54 mol H<sup>+</sup> kg<sup>-1</sup>  
260 solid). The alkaline groups decreased slowly over time, which may be attributed to the transformation or  
261 dissolution of alkaline minerals (hydrogarnet, calcite, sodalite) during weathering. In addition, disposal  
262 promotes a decrease in fine grains and the formation of macro-aggregates (Figure 3), whilst resulting in  
263 reduction of the specific surface area; these changes affect the distribution of alkaline groups on particle  
264 surfaces. Furthermore, precipitation of amorphous and semi-amorphous minerals accelerates this behavior,  
265 and improvement of these minerals with structural defects determine the intraparticle diffusion that allow  
266 the surface adsorbed alkaline groups to re-distribute (Castaldi *et al.*, 2008; Wu *et al.*, 2009; Clark *et al.*,  
267 2011). Further to this, the alkaline group behavior may enhance the development of alkaline minerals in  
268 bauxite residue following disposal.

#### 269 *Potential implications for soil formation and land development at BRDAs*

270 Bauxite residues have multiple chemical and physical limitations that require amelioration prior to  
271 forming a stable soil structure and land substrate to support plant growth. High alkalinity and complex  
272 alkaline minerals appear to mainly restrain land development and rehabilitation on BRDAs.  
273 Environmental management of BRDAs have commonly focused on containment and alkalinity



274 neutralized or removed by artificial trials (Courtney *et al.*, 2009; Smart *et al.*, 2016; Goloran *et al.*, 2017),  
275 with less attention given to long term evolution of the electrochemical properties of alkalinity following  
276 disposal, particularly soil formation and further land development. Currently, almost all BRDAs in China  
277 are left to natural weathering processes (Zhu *et al.*, 2016b; Zhu *et al.*, 2016c). Environmental plans are  
278 gradually moving to amelioration and soil formation to reduce environmental risks and occupied land  
279 degradation, and subsequently establish a stable ecosystem. This study has demonstrated that reduction of  
280 alkalinity within bauxite residue is closely related to changes in mineralogy, zeta potential, bulk IEP,  
281 surface protonation and alkaline groups. With increasing duration following disposal, transformations or  
282 dissolution of hydrogarnet, cancrinite, sodalite and calcite, and a decrease in IEP and alkaline groups, the  
283 alkalinity of residue decreases.

284 Understanding the influences of bauxite residue mineralogy on the proton adsorption behavior is  
285 important in relation to environmental issues of BRDAs. Complex mineralogy often dominates residue  
286 disposal areas, leading to long term leakage of alkaline compounds, alkalization and/or degradation of  
287 occupied land, and diffusion and/or overflow of alkaline dust and efflorescence substances formed at the  
288 surface of BRDAs during storm events (Courtney & Harrington, 2012; Santini & Fey, 2015; Higgins *et al.*,  
289 2016; Higgins *et al.*, 2017; Zhu *et al.*, 2017). Therefore, understanding the effects of different disposal  
290 years on bauxite residue mineralogy, and the influences of mineralogy on proton adsorption behavior of  
291 bauxite residue, highlight the requirement for effective environmental management of BRDAs.  
292 Furthermore, surface electrochemical characteristics following disposal are an important step in the  
293 transformation of alkaline substances and a reduction in the alkaline properties, especially surface  
294 alkaline groups, which may further increase the rate of soil formation and land development (Xue *et al.*  
295 2016b).

296 Disposal duration significantly improves surface alkaline electrochemical characteristics of bauxite  
297 residue whilst ameliorating some physical properties (fine grains reduced and macro-aggregates formed)  
298 in respect to soil formation at the surface of BRDAs'. A decrease in IEP and alkaline groups have a  
299 positive effect on improving physical properties, releasing a novel signal that soil formation and  
300 rehabilitation of BRDAs may achieve with disposal duration, but the evidences are insufficient only  
301 concentrating on macro-aggregate formations. Future investigations should focus on the increasing  
302 physical limitations (aggregate structural formation, resistance to erosion, water holding characteristics),  
303 whilst questioning the interactions between electrochemistry and soil development of bauxite residue  
304 following long-term natural weathering, finally forming a land surface and achieving rehabilitation on  
305 BRDAs.

306

## CONCLUSION

307 This paper presents evidence of changes in surface electrochemical characteristics of alkalinity within  
308 bauxite residue following long term disposal. Transformation of alkaline minerals of calcite, hydrogarnet  
309 and sodalite occur over time and their concentrations decrease by approximately 20 % after a 20 year  
310 duration following disposal. Some amorphous and semi-amorphous minerals in the 20 year old residue  
311 decreased by 10 % with a corresponding decrease in BET surface area and sorption sites. Alkaline  
312 minerals and amorphous minerals are responsible for the magnitude and range of zeta potential curves.  
313 Dissolution of hydrogarnet and sodalite appear to greatly affect IEP shifts, significantly reducing the IEP.  
314 Over time (20 years) there was a reduction in alkaline mineral concentrations but also the improvement of

315 the poorly electrostatic and crystalline structures of amorphous and semi-amorphous minerals, reduced  
316 surface protonation and a 47 % reduction in surface active alkaline groups. These findings are significant  
317 as they help to understand the effects of mineralogy on adsorption behavior in bauxite residue, and benefit  
318 decision making with regards to degradation of occupied land, soil formation and land development of  
319 BRDAs.

320

## ACKNOWLEDGEMENTS

321 This project was funded by the National Natural Science Foundation of China (Grant No. 41371475), the  
322 Environmental Protection's Special Scientific Research for Chinese Public Welfare Industry (Grant No.  
323 201509048), and the Innovative Project of Independent Exploration for PhD of Central South University  
324 (Grant No. 2016zzts036). The authors sincerely acknowledge the anonymous reviewers for their insights  
325 and comments to further improve the quality of the manuscript.

326

327

## REFERENCES

- 328 Axe L, Trivedi P. 2002. Intraparticle surface diffusion of metal contaminants and their attenuation in microporous amorphous Al, Fe,  
329 and Mn oxides. *Journal of Colloid & Interface Science* **247**: 259-265. DOI:10.1006/jcis.2001.8125.
- 330 Barnes MC, Addai-Mensah J, Gerson AR. 1999. The kinetics of desilication of synthetic spent Bayer liquor seeded with cancrinite  
331 and cancrinite/sodalite mixed-phase crystals. *Journal of Crystal Growth* **200**: 251-264. DOI:10.1016/S0022-0248(98)01294-9.
- 332 Buckley R, Curtin T, Courtney R. 2016. The potential for constructed wetlands to treat alkaline bauxite residue leachate: Laboratory  
333 investigations. *Environmental Science & Pollution Research* **23**: 14115-14122. DOI:10.1007/s11356-016-6582-8.
- 334 Burke IT, Peacock CL, Lockwood CL, Stewart DI, Mortimer RJG, Ward MB, Renforth P, Gruiz K, Mayes WM. 2013. Behavior of  
335 Aluminum, Arsenic, and Vanadium during the neutralization of red mud leachate by HCl, gypsum, or seawater. *Environmental*  
336 *Science & Technology* **12**: 6527-6535. DOI:10.1021/es4010834.
- 337 Castaldi P, Santona L, Enzo S, Melis P. 2008. Sorption processes and XRD analysis of a natural zeolite exchanged with Pb<sup>2+</sup>, Cd<sup>2+</sup>  
338 and Zn<sup>2+</sup> cations. *Journal of Hazardous Materials* **156**: 428-434. DOI:10.1016/j.jhazmat.2007.12.040.
- 339 Castaldi P, Silveti M, Garau G, Deiana S. 2010. Influence of the pH on the accumulation of phosphate by red mud (a bauxite ore  
340 processing waste). *Journal of Hazardous Materials* **182**: 266-272. DOI:10.1016/j.jhazmat.2010.06.025.
- 341 Clark M, Berry J, Mcconchie D. 2009. The long-term stability of a metal-laden Bauxsol™ reagent under different geochemical  
342 conditions. *Geochemistry Exploration Environment Analysis* **9**: 101-112. DOI:10.1144/1467-7873/07-164.
- 343 Clark MW, Harrison JJ, Payne TE. 2011. The pH-dependence and reversibility of uranium and thorium binding on a modified  
344 bauxite refinery residue using isotopic exchange techniques. *Journal of Colloid & Interface Science* **356**: 699-705.  
345 DOI:10.1016/j.jcis.2011.01.068.
- 346 Clark MW, Johnston M, Reichelt-Brushett AJ. 2015. Comparison of several different neutralisations to a bauxite refinery residue:  
347 Potential effectiveness environmental ameliorants. *Applied Geochemistry* **56**: 1-10. DOI:10.1016/j.apgeochem.2015.01.015.
- 348 Costanza R, Groot RD, Sutton P, Ploeg SVD, Anderson SJ, Kubiszewski I, Farber S, Turner RK. 2014. Changes in the global value  
349 of ecosystem services. *Global Environmental Change* **26**: 152-158. DOI:10.1016/j.gloenvcha.2014.04.002.
- 350 Couperthwaite SJ, Johnstone DW, Millar GJ, Frost RL. 2013. Neutralization of acid sulfate solutions using bauxite refinery residues  
351 and its derivatives. *Industrial & Engineering Chemistry Research* **52**: 1388-1395. DOI:10.1021/ie301618p.
- 352 Courtney R, Harrington T. 2012. Growth and nutrition of *Holcus lanatus* in bauxite residue amended with combinations of spent  
353 mushroom compost and gypsum. *Land Degradation & Development* **23**: 144-149. DOI:10.1002/ldr.1062.
- 354 Courtney RG, Jordan SN, Harrington T. 2009. Physico-chemical changes in bauxite residue following application of spent

355 mushroom compost and gypsum. *Land Degradation & Development* **20**: 572-581. DOI:10.1002/ldr.926.

356 Davis JA, Kent DB. 1990. Surface complexation modeling in aqueous geochemistry. *Reviews in Mineralogy* **23**: 177-260.

357 Evans K. 2016. The history, challenges, and new developments in the management and use of bauxite residue. *Journal of*

358 *Sustainable Metallurgy* **2**: 316-331. DOI:10.1007/s40831-016-0060-x.

359 Freire TSS, Clark MW, Comarmond MJ, Payne TE, Reichelt-Brushett AJ, Thorogood GJ. 2012. Electroacoustic isoelectric point

360 determinations of bauxite refinery residues: Different neutralization techniques and minor mineral effects. *Langmuir* **28**:

361 11802-11811. DOI:10.1021/la301790v.

362 Gatta GD, Lotti P, Kahlenberg V, Haefeker U. 2016. The low-temperature behaviour of cancrinite: an in situ single-crystal X-ray

363 diffraction study. *Mineralogical Magazine* **76**: 933-948. DOI: 10.1180/minmag.2012.076.4.10.

364 Gelencser A, Kovats N, Turoczi B, Rostasi A, Hoffer A, Imre K, Nyiro-Kosa I, Csakberenyi-Malasics D, Toth A, Czitrovsky A,

365 Nagy A, Nagy S, Acs A, Kovacs A, Ferincz A, Hartanyi Z, Posfai M. 2011. The red mud accident in Ajka (Hungary):

366 Characterization and potential health effects of fugitive dust. *Environmental Science & Technology* **45**: 1608-1615.

367 DOI:10.1021/es104005r.

368 Genç-Fuhrman H, Tjell JC, McConchie D. 2004. Adsorption of arsenic from water using activated neutralized red mud.

369 *Environmental Science & Technology* **38**: 2428-2434. DOI:10.1021/es035207h.

370 Genç-Fuhrman H, Tjell JC, McConchie D. 2004. Increasing the arsenate adsorption capacity of neutralized red mud (Bauxsol).

371 *Journal of Colloid and Interface Science* **271**: 313-320. DOI:10.1016/j.jcis.2003.10.011.

372 Goloran JB, Phillips IR, Chen CR. 2017. Forms of nitrogen alter plant phosphorus uptake and pathways in rehabilitated highly

373 alkaline bauxite processing residue sand. *Land Degradation & Development* **28**: 628-637. DOI:10.1002/ldr.2630.

374 Gong XY, Nie ZM, Qian MX, Liu J, Pedesron LA, Hobbs DT, McDuffie NG. 2003. Gibbsite to boehmite transformation in strongly

375 caustic and nitrate environments. *Industrial & Engineering Chemistry Research* **42**. DOI:10.1021/ie020837y.

376 Grafe M, Power G, Klauber C. 2011. Bauxite residue issues: III. Alkalinity and associated chemistry. *Hydrometallurgy* **108**: 60-79.

377 DOI:10.1016/j.hydromet.2011.02.004.

378 Hawkins DB, Roy R. 1963. Experimental hydrothermal studies on rock alteration and clay mineral formation. *Geochimica Et*

379 *Cosmochimica Acta* **27**: 1047-1054. DOI:10.1016/0016-7037(63)90065-6.

380 Higgins D, Curtin T, Courtney R. 2017. Effectiveness of a constructed wetland for treating alkaline bauxite residue leachate: a

381 1-year field study. *Environmental Science & Pollution Research* **24**: 8516-8524. DOI:10.1007/s11356-017-8544-1.

382 Higgins D, Curtin T, Pawlett M, Courtney R. 2016. The potential for constructed wetlands to treat alkaline bauxite-residue leachate:

383 Phragmites australis growth. *Environmental Science & Pollution Research* **23**: 24305-24315. DOI:10.1007/s11356-016-7702-1.

384 Jimenez-Angeles F. 2012. Effects of mixed discrete surface charges on the electrical double layer. *Physical Review E Statistical*

385 *Physics Plasmas Fluids & Related Interdisciplinary Topics* **86**: 1818-1834. DOI:10.1103/PhysRevE.86.021601.

386 Jones BEH, Haynes RJ, Phillips IR. 2015. Influence of amendments on acidification and leaching of Na from bauxite processing

387 sand. *Ecological Engineering* **84**: 435-442. DOI:10.1016/j.ecoleng.2015.09.054.

388 Kairies CL, Capo RC, Watzlaf GR. 2005. Chemical and physical properties of iron hydroxide precipitates associated with passively

389 treated coal mine drainage in the Bituminous Region of Pennsylvania and Maryland. *Applied Geochemistry* **20**: 1445-1460.

390 DOI:10.1016/j.apgeochem.2005.04.009.

391 Kinnarinen T, Holliday L, Häkkinen A. 2015. Dissolution of sodium, aluminum and caustic compounds from bauxite residues.

392 *Minerals Engineering* **79**: 143-151. DOI:10.1016/j.mineng.2015.06.007.

393 Kishida M, Harato T, Tokoro C, Owada S. 2016. In situ remediation of bauxite residue by sulfuric acid leaching and

394 bipolar-membrane electrodialysis. *Hydrometallurgy*. DOI:10.1016/j.hydromet.2016.04.012.

395 Kong XF, Guo Y, Xue SG, Hartley W, Wu C, Ye YZ, Cheng QY. 2017b. Natural evolution of alkaline characteristics in bauxite

396 residue. *Journal of Cleaner Production* **143**: 224-230. DOI:10.1016/j.jclepro.2016.12.125.

397 Kong XF, Li M, Xue SG, Hartley W, Chen CR, Wu C, Li XF, Li YW. 2017a. Acid transformation of bauxite residue: Conversion of

398 its alkaline characteristics. *Journal of Hazardous Materials* **324**: 382-390. DOI:10.1016/j.jhazmat.2016.10.073.

399 Kosmulski M. 2014. The pH dependent surface charging and points of zero charge. VI. Update. *Journal of Colloid & Interface*

400 *Science* **426**: 209-212. DOI:10.1016/j.jcis.2014.02.036.

401 Liao CZ, Zeng LM, Shih KM. 2015. Quantitative X-ray Diffraction (QXRD) analysis for revealing thermal transformations of red

402 mud. *Chemosphere* **131**: 171-177. DOI:10.1016/j.chemosphere.2015.03.034.

403 Liu WC, Chen XQ, Li WX, Yu YF, Yan K. 2014. Environmental assessment, management and utilization of red mud in China.

404 *Journal of Cleaner Production* **84**: 606-610. DOI:10.1016/j.jclepro.2014.06.080.

405 Liu Y, Naidu R. 2014. Hidden values in bauxite residue (red mud): Recovery of metals. *Waste Management* **34**: 2662-2673.

406 DOI:10.1016/j.wasman.2014.09.003.

407 Liu Y, Naidu R, Ming H. 2013. Surface electrochemical properties of red mud (bauxite residue): Zeta potential and surface charge

408 density. *Journal of Colloid and Interface Science* **394**: 451-457. DOI:10.1016/j.jcis.2012.11.052.

409 Mayes WM, Burke IT, Gomes HI, Anton AD, Molnár M, Feigl V, Ujaczki É. 2016. Advances in understanding environmental risks

410 of red mud after the Ajka Spill, Hungary. *Journal of Sustainable Metallurgy* **2**: 332-343. DOI:10.1007/s40831-016-0050-z.

411 Murray J, Kirwan L, Loan M, Hodnett BK. 2009. In-situ synchrotron diffraction study of the hydrothermal transformation of

412 goethite to hematite in sodium aluminate solutions. *Hydrometallurgy* **95**: 239-246. DOI:10.1016/j.hydromet.2008.06.007.

413 Palmer SJ, Frost RL. 2011. Characterization of bayer hydrotalcites formed from bauxite refinery residue liquor. *Industrial &*

414 *Engineering Chemistry Research* **50**: 5346-5351. DOI:10.1021/ie1018194.

415 Pan X, Yu H, Tu G. 2015. Reduction of alkalinity in bauxite residue during Bayer digestion in high-ferrite diasporic bauxite.

416 *Hydrometallurgy* **151**: 98-106. DOI:10.1016/j.hydromet.2014.11.015.

417 Rai SB, Wasewar KL, Mishra RS, Mahindran P, Chaddha MJ, Mukhopadhyay J, Yoo C. 2013. Sequestration of carbon dioxide in

418 red mud. *Desalination and Water Treatment* **51**: 2185-2192. DOI:10.1080/19443994.2012.734704.

419 Samal S, Ray AK, Bandopadhyay A. 2015. Characterization and microstructure observation of sintered red mud - fly ash mixtures

420 at various elevated temperature. *Journal of Cleaner Production* **101**: 368-376. DOI:10.1016/j.jclepro.2015.04.010.

421 Santini TC, Fey MV, Gilkes RJ. 2015. Experimental simulation of long term weathering in alkaline bauxite residue tailings. *Metals*

422 **5**: 1241-1261. DOI:10.3390/met5031241.

423 Santini TC, Banning NC. 2016. Alkaline tailings as novel soil forming substrates: Reframing perspectives on mining and refining

424 wastes. *Hydrometallurgy* **164**: 38-47. DOI:10.1016/j.hydromet.2016.04.011.

425 Santini TC, Fey MV. 2015. Fly ash as a permeable cap for tailings management: Pedogenesis in bauxite residue tailings. *Journal of*

426 *Soils and Sediments* **15**: 552-564. DOI:10.1007/s11368-014-1038-6.

427 Sharif MSU, Davis RK, Steele KF, Kim B, Hays PD, Kresse TM, Fazio JA. 2011. Surface complexation modeling for predicting

428 solid phase arsenic concentrations in the sediments of the Mississippi River Valley alluvial aquifer, Arkansas, USA. *Applied*

429 *Geochemistry* **26**: 496-504. DOI:10.1016/j.apgeochem.2011.01.008.

430 Smart D, Callery S, Courtney R. 2016. The potential for waste-derived materials to form soil covers for the restoration of mine

431 tailings in Ireland. *Land Degradation & Development* **27**: 542-549. DOI:10.1002/ldr.2465.

432 Smičiklas I, Smiljanić S, Perić-Grujić A, Šljivić-Ivanović M, Mitrić M, Antonović D. 2014. Effect of acid treatment on red mud

433 properties with implications on Ni(II) sorption and stability. *Chemical Engineering Journal* **242**: 27-35.

434 DOI:10.1016/j.cej.2013.12.079.

435 Snars K, Gilkes RJ. 2009. Evaluation of bauxite residues (red muds) of different origins for environmental applications. *Applied*

436 *Clay Science* **46**: 13-20. DOI:10.1016/j.clay.2009.06.014.

437 Sushil S, Batra VS. 2012. Modification of red mud by acid treatment and its application for CO removal. *Journal of Hazardous*

438 *Materials* **203-204**: 264-273. DOI:10.1016/j.jhazmat.2011.12.007.

439 Sutton PC, Anderson SJ, Costanza R, Kubiszewski I. 2016. The ecological economics of land degradation: Impacts on ecosystem

440 service values. *Ecological Economics* **129**: 182-192. DOI:10.1016/j.ecolecon.2016.06.016.

441 Tsuchida T. 2000. Hydrothermal synthesis of submicrometer crystals of boehmite. *Journal of the European Ceramic Society* **20**:  
442 1759-1764. DOI:10.1016/S0955-2219(00)00052-2.

443 Tuazon D, Corder GD. 2008. Life cycle assessment of seawater neutralised red mud for treatment of acid mine drainage. *Resources,*  
444 *Conservation and Recycling* **52**: 1307-1314. DOI:10.1016/j.resconrec.2008.07.010.

445 Wang Y, Ye L, Hu Y. 2008. Adsorption mechanisms of Cr(VI) on the modified bauxite tailings. *Minerals Engineering* **21**: 913-917.  
446 DOI:10.1016/j.mineng.2008.04.003.

447 Wong JWC, Ho GE. 1993. Use of waste gypsum in the revegetation on red mud deposits: A greenhouse study. *Waste Management*  
448 *& Research* **11**: 249-256. DOI:10.1006/wmre.1993.1024.

449 Wong JWC, Ho GE. 1994. Effectiveness of acidic industrial wastes for reclaiming fine bauxite refining residue (red mud). *Soil*  
450 *Science* **158**: 115-123. DOI:10.1097/00010694-199408000-00005.

451 Wu FC, Tseng RL, Juang RS. 2009. Initial behavior of intraparticle diffusion model used in the description of adsorption kinetics.  
452 *Chemical Engineering Journal* **153**: 1-8. DOI:10.1016/j.cej.2009.04.042.

453 Xue SG, Kong XF, Zhu F, Hartley W, Li XF, Li YW. 2016a. Proposal for management and alkalinity transformation of bauxite  
454 residue in China. *Environmental Science & Pollution Research* **23**: 12822-12834. DOI:10.1007/s11356-016-6478-7.

455 Xue SG, Zhu F, Kong XF, Wu C, Huang L, Huang N, Hartley W. 2016b. A review of the characterization and revegetation of  
456 bauxite residues (Red mud). *Environmental Science & Pollution Research* **23**: 1120-1132. DOI:10.1007/s11356-015-4558-8.

457 Yang JJ, Li JW, Xiao YL, Luo ZT, Han YF. 2012. Research on dealkalization of sintering process red mud by lime process at  
458 normal atmosphere and mechanism theory. *Inorganic Chemicals Industry* **44**: 40-42. (in Chinese)

459 Ye N, Yang JK, Ke X, Zhu J, Li YL, Xiang C, Wang HB, Li L, Xiao B. 2014. Synthesis and characterization of Geopolymer from  
460 Bayer red mud with thermal pretreatment. *Journal of the American Ceramic Society* **97**: 1652-1660. DOI:10.1111/jace.12840.

461 Zhu F, Hou JT, Xue SG, Wu C, Wang QL, Hartley W. 2017. Vermicompost and gypsum amendments improve aggregate formation  
462 in bauxite residue. *Land Degradation & Development*. DOI:10.1002/ldr.2737.

463 Zhu F, Liao JX, Xue SG, Hartley W, Zou Q, Wu H. 2016c. Evaluation of aggregate microstructures following natural regeneration  
464 in bauxite residue as characterized by synchrotron-based X-ray micro-computed tomography. *Science of the Total Environment*  
465 **573**: 155-163. DOI:10.1016/j.scitotenv.2016.08.108.

466 Zhu F, Xue SG, Hartley W, Huang L, Wu C, Li XF. 2016a. Novel predictors of soil genesis following natural weathering processes  
467 of bauxite residues. *Environmental Science & Pollution Research* **23**: 2856-2863. DOI:10.1007/s11356-015-5537-9.

468 Zhu F, Zhou JY, Xue SG, Hartley W, Wu C, Guo Y. 2016b. Aging of bauxite residue in association of regeneration: A comparison  
469 of methods to determine aggregate stability & erosion resistance. *Ecological Engineering* **92**: 47-54. DOI:10.1016/j.ecoleng.  
470 2016.03.025.

471 Zhu XB, Li W, Guan XM. 2015. An active dealkalization of red mud with roasting and water leaching. *Journal of Hazardous*  
472 *Materials* **286**: 85-91. DOI:10.1016/j.jhazmat.2014.12.048.

473

474

475

476

477

478

479

480

481

482

483

484  
485  
486  
487  
488  
489  
490

491 Table I. Mineral composition of bauxite residue following its long-term disposal.

Mineral phase			Disposal years				
Name	Formula	units	Fresh	5	10	15	20
Calcite	CaCO <sub>3</sub>	%	10.0	10.2	9.7	8.9	8.2
Cancrinite	Na <sub>8</sub> Al <sub>6</sub> Si <sub>6</sub> O <sub>24</sub> (CO <sub>3</sub> )(H <sub>2</sub> O) <sub>2</sub>	%	3.6	3.6	3.5	3.6	3.8
Diaspore	α-AlOOH	%	5.9	6.1	6.0	5.8	5.9
Gibbsite	Al(OH) <sub>3</sub>	%	- <sup>a</sup>	2.4	4.7	7.1	8.9
Hydrogarnet	Ca <sub>3</sub> Al <sub>2</sub> (SiO <sub>4</sub> ) <sub>x</sub> (OH) <sub>12-4x</sub>	%	20.2	19.8	18.1	17.5	16.2
Sodalite	Na <sub>8</sub> Al <sub>6</sub> Si <sub>6</sub> O <sub>24</sub> Cl <sub>2</sub>	%	12.2	11.7	10.9	10.1	9.5
TCA <sup>b</sup>	Ca <sub>3</sub> Al <sub>2</sub> (OH) <sub>12</sub>	%	5.5	5.4	5.2	5.3	5.2
Hematite	α-Fe <sub>2</sub> O <sub>3</sub>	%	26.3	26.4	26.2	25.8	26.0
Perovskite	Ca(TiO <sub>3</sub> )	%	12.6	12.3	12.4	12.2	12.2
Quartz	SiO <sub>2</sub>	%	2.5	2.9	3.3	3.7	4.1
Amorphous mineral		%	62.8±1	60.9±1	59.1±1	57.7±1	56.3±1
Semi-amorphous mineral		%	22.4±0.6	21.9±0.5	21.6±0.5	21.0±0.4	20.3±0.5
BET surface area		m <sup>2</sup> /g	8.84	8.16	7.78	7.09	6.32
Estimated sorption site <sup>c</sup>		μmol/g	33.95	31.33	29.88	27.23	26.27

<sup>a</sup>Gibbsite may exist in the fresh bauxite residue, but the mineral content lowers the detection limit of X-ray powder diffraction.

<sup>b</sup>TCA: Tri-calcium aluminate.

<sup>c</sup>Estimation of sorption site is calculated by the standard value of 3.84 μmol/m<sup>2</sup> derived from Davis and Kent (Davis & Kent, 1990).

492